analytical chemistry

pubs.acs.org/ac
Article

A Reversible ATR-FTIR Biosensor with Single-Residue Sensitivity

Adrian Höveler,[§] Marvin Mann,[§] Maiko Czarnetzki, Jonas Simon, Nicolai Marpert, Jörn Güldenhaupt, Klaus Gerwert, and Carsten Kötting*

Cite This: *Anal. Chem.* 2026, 98, 11935−11943
Read Online

ABSTRACT: Infrared spectroscopy provides label-free access to protein structure information with high sensitivity. Challenges in infrared spectroscopy include artifacts arising from temperature changes, baseline drifts, and the strong water absorption, especially in difference spectroscopy, where signals are orders of magnitude smaller than the total absorbance. Previously, we introduced an ATR-based immuno-infrared sensor (iRS) based on sophisticated surface chemistry. This provides a stable platform for covalent protein immobilization and allows its application with body fluids such as cerebrospinal fluid or blood without unspecific background. It detects misfolding of small amounts of antigen (Aβ or α-synuclein) by binding to an antibody or antibody fragment, which allows for the diagnosis of various neurodegenerative diseases. Here, we extend this platform by introducing reversible binding via the NColE7/Im7 pair. Im7-tagged proteins are captured with subpicomolar affinity and quantitatively released under mild conditions (high salt or low pH), allowing repeated capture-regeneration cycles with continuous spectral monitoring of the Im7 fusion protein. Using an Im7-antibody Fab fusion protein, we present a reusable immuno-IR sensor that enables multiple measurements on the same surface. For example, different antibodies can be used for differential screening. Using alternating Im7 protein attachments to the internal reflection element, we further compare Im7 single point mutants to wild-type Im7 to resolve infrared signatures of specific amino acid substitutions. Difference spectra reveal the distinct tyrosine absorption associated with either the introduction or removal of a single tyrosine residue, providing a proof-of-concept for single-residue sensitivity in infrared difference spectroscopy enabled by complete protein exchange instead of induced perturbations on the same protein.

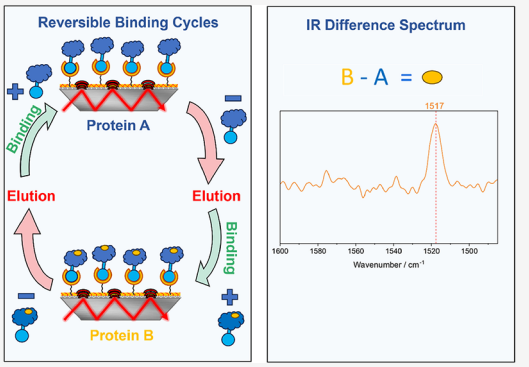

INTRODUCTION

Infrared (IR) spectroscopy is a versatile technique with multiple applications in protein analysis.[1,2] One application is based on the amide I mode, which is sensitive to secondary structure and provides a straightforward method for studying protein folding processes.[3] This principle is used in recent biosensors for diagnostics of neurodegenerative diseases such as Alzheimer's disease[4−6] or Parkinson's diseases.[7,8] Another important approach is infrared difference spectroscopy. This method can be used to elucidate reaction mechanisms.[1,9−11] By subtracting spectra of two defined protein states, structural changes on the level of single functional groups become detectable. All absorptions that do not change during the reaction are canceled out, leaving only the signal of the groups involved in the reaction. However, difference signals are typically about 10^3 times smaller than the total absorbance, making them extremely sensitive to even minor variations in hydration, baseline drifts, protein orientation or temperature. For this reason, reactions must be performed within the spectrometer under precise temperature control, often triggered by a rapid perturbation such as a laser flash. Further possibilities arise when using proteins immobilized on an ATR crystal.[12,13] Here, difference spectroscopy can be initiated by change of buffer, binding of ligands or even other proteins.[14,15] ATR-FTIR difference spectroscopy therefore requires (i) exceptional surface stability, (ii) reproducible and uniform immobilization geometry and (iii) minimal run-to-run drift.[1,10] Here we present a method to obtain difference spectra from two independent samples and reach atomic resolution for this type of measurement, based on subμg samples. To our knowledge, such sensitivity has not been achieved previously.

Our iRS setup is based on a patented surface chemistry,[16,17] here combined with a reversible affinity tag. Reversible biosensing systems have become essential tools in modern biophysical and analytical chemistry, enabling the detailed kinetic and structural analysis of biomolecular interactions. Surface plasmon resonance (SPR) and related label free techniques have long relied on reversible affinity tags and regeneration cycles to obtain reproducible, quantitative data

Received: January 12, 2026
Revised: March 12, 2026
Accepted: March 16, 2026
Published: April 16, 2026

https://doi.org/10.1021/acs.analchem.6c00250
Anal. Chem. 2026, 98, 11935−11943

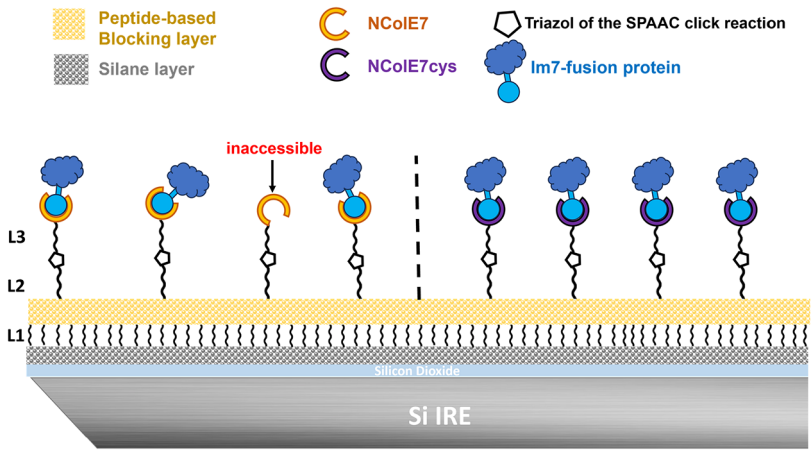

Figure 1. Schematic representation of the iRS with a reversible REoB surface (Recognition Element on a covalently attached Blocking layer) on which the bacterial nuclease NColE7 has been covalently attached as a biological recognition element. NColE7 is covalently attached via strain-promoted azide−alkyne cycloaddition to a silicon crystal that has been previously functionalized with azide silanes and a peptide-blocking layer.[33] Surface-bound NColE7 subsequently serves as a high-affinity capture module for Im7 fusion proteins (e.g., IM7 fused with a Fab fragment). Left panel: In nonoriented coupling, a fraction of NColE7 (orange) molecules may adopt suboptimal orientations that are inaccessible for Im7 binding. Right panel: Optimized surface design with site-specific NColE7cys labeling to achieve oriented attachment to the surface.

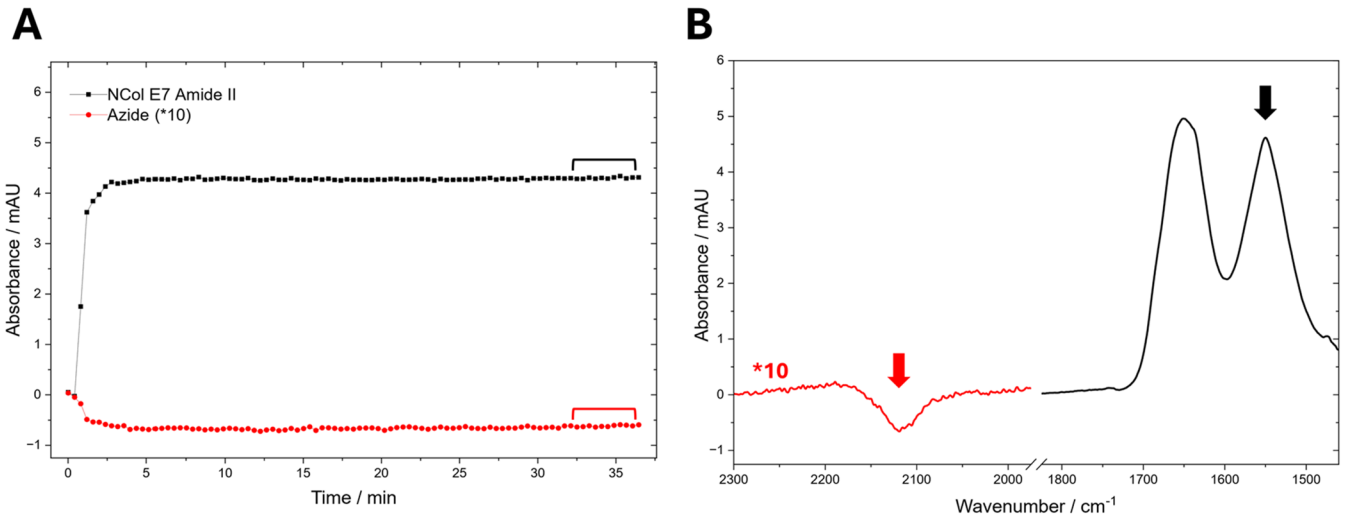

Figure 2. Immobilization of DBCO-NColE7 on a covalently blocked sensor surface modified with azide groups. (A) Kinetics of Amide II absorbance of NColE7 binding (black) and the corresponding kinetics of the azide band (red, magnified by a factor of 10 for clarity). After 30 min of immobilization, 4 mAU of NColE7 are bound and 0.1 mAU of azide are consumed from the surface. (B) Averaged spectra from the end of the NColE7 surface immobilization (indicated by brackets in A). The immobilization of NColE7 is observed by an increase in the amide I and amide II bands. The amount of azide linker that has reacted can be observed by a negative band at 2100 cm^{-1}. The azide band region (red) is magnified by a factor of 10.

across multiple binding events. In contrast to single-use immunoassays, reversible systems allow direct comparability across sequential immobilizations and avoid sensitivity to surface-to-surface variability in a time- and material-efficient manner.[18,19]

Reversible affinity systems commonly used in biosensing include well-established pairs such as biotin streptavidin, His-tag Ni-NTA or Protein A/G.[20−22] However, these systems typically suffer from limited reversibility, harsh regeneration conditions, or insufficient affinity,[23] which degrade the capture layer by reducing capacity and increasing heterogeneity over cycles.[24,25]

Among reversible affinity systems, the DNase domain of *Escherichia coli* colicin E7 (NColE7) with its cognate immunity protein Im7 stands out. The NColE7-Im7 complex exhibits subpicomolar affinity (K_d∼10^{-14} M), rapid association kinetics, and strong electrostatic and shape complementarity, while both proteins tolerate substantial engineering without loss of structural integrity.[26−28] Its suitability for repeated biosensing was demonstrated by Hosse et al.,[29] who showed 40 capture−regeneration cycles with <2% loss of activity on a Biacore CM5 chip. Further implementations include use for affinity chromatography and ATR immobilization of Im7-labeled antibody fragments, enabling spectroscopic characterization of proteins.[30−32] It provides the chemical stability and mild regeneration conditions needed to obtain reproducible ATR-FTIR spectra and reliable difference spectra across repeated binding events, opening the route toward quantitatively comparing antibody constructs, protein variants, and even subtle structural differences such as point mutations under identical interfacial conditions.

https://doi.org/10.1021/acs.analchem.6c00250
Anal. Chem. 2026, 98, 11935−11943

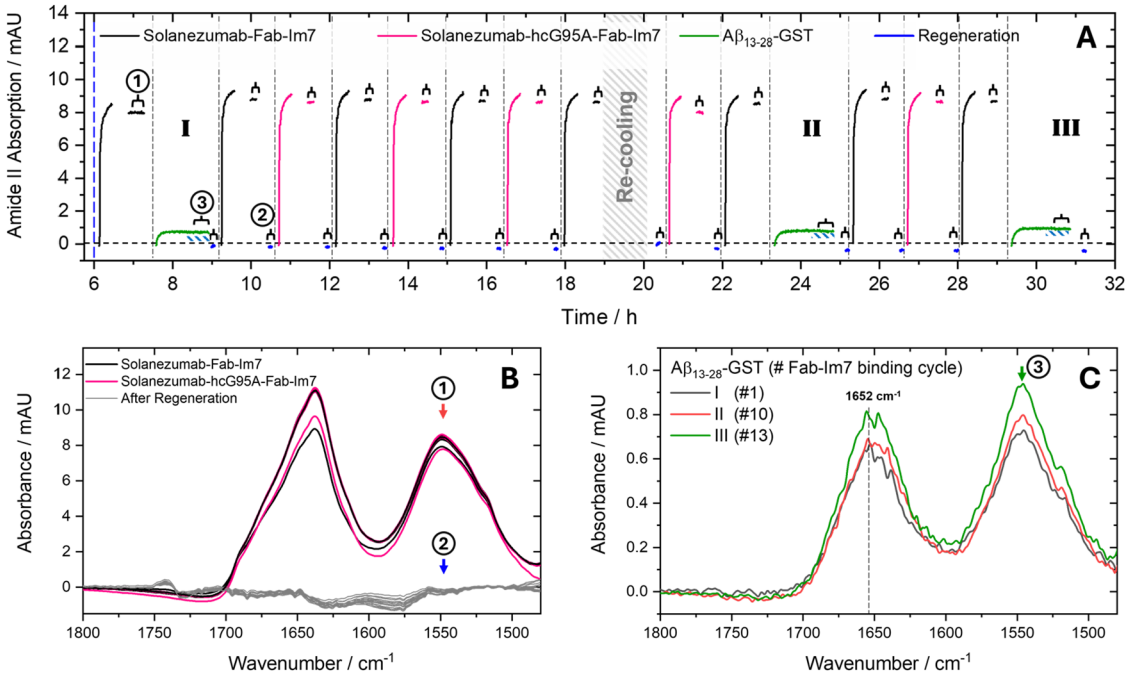

Figure 3. Illustration of the capabilities of a reversible ATR-FTIR surface. (A) The kinetics of the amide II band during several binding and regeneration cycles of two different Im7-Fab fusion proteins. Solanezumab-Im7 (black) and solanezumab-Im7 inactive mutant (G95A, pink) were alternately bound. Thirteen cycles were recorded, with no detectable loss of reusability of the NColE7 capturing surface. A constant amount of Im7 fusion protein could be bound (8 mAU), regardless of which fusion protein was used. After the first, 10th, and 13th binding cycle, an activity test was performed using GST-Aß13−28 (green) as the solanezumab antigen, respectively. (B) Spectra of the Im7-Fab fusion proteins from all 13 cycles. Im7 is consistently and uniformly attached (1). After each cycle, a 20-min regeneration step with 3.5 M $MgCl_2$ was performed, and the spectrum was recorded (2). Always, the Im7 fusion protein was completely eluted, and the surface showed no visible protein remnants. (C) The antigen spectra of GST-Aß13-28 (3) after the first, 10th, and 13th cycle are shown. Even after hours of use of the surface and regeneration, the antigen can be measured as reproduced. The performance of the Im7 fusion proteins remained unchanged throughout.

RESULTS AND DISCUSSION

Reversible Infrared Sensor

The setup used throughout this study is shown in Figure 1. The patented surface architecture[16,17] was introduced for the application of an immuno-IR sensor (iRS).[33] Here, the method is extended in two ways: (i) the NColE7-Im7 system is used as a reversible tag, allowing for repeated stable immobilization and complete wash off of the molecule of interest and (ii) we use the reversibility of the system for an enhanced difference spectroscopy method.

The reversible infrared biosensor is based on a REoB (Recognition Element on covalently attached Blocking layer) architecture, which is built directly onto the silicon ATR crystal. The silicon dioxide surface was first functionalized with a silane layer, which provided reactive groups for subsequent modification. In a second step, a peptide-based blocking layer was covalently attached to this silanized surface to prevent nonspecific protein adsorption. A second linker adds reactive azide groups to the peptide-based blocking layer.

To enable reversible binding of Im7-tagged proteins to this surface, NColE7 was modified with DBCO groups using a DBCO-NHS linker. The coupling efficiency can be controlled by pH, time, and temperature and was adjusted to yield 1.91 ± 0.87 (n = 16) DBCO groups per NColE7 as determined by matrix-assisted laser desorption ionization (MALDI) mass spectrometry (Figure S1) and UV/vis spectroscopy (Figure S2). The modifications are not site-directed and are expected to be distributed among the 33 lysine residues and the N-terminus of NColE7. Two of these lysines (K525 and K528) are located within the interaction site of NColE7-Im7. NColE7 molecules that have been DBCOylated in these positions will interfere with the Im7 binding (Figure S1).

The DBCO-modified NColE7 was then immobilized onto the azide group-containing ATR surface via strain-promoted azide−alkyne cycloaddition (SPAAC). The immobilization kinetics are shown in Figure 2A. The amide II signal increases rapidly and reaches a plateau at approximately 4 mAU after about 5 min. Simultaneously, the azide band at ∼2100 cm^{-1} decreases by ∼0.1 mAU, demonstrating consumption of azide groups, confirming that immobilization proceeds through the intended SPAAC reaction. The end point spectrum (Figure 2B) displays the characteristic amide I/II bands of a protein layer, together with a strongly diminished azide signal. The parallel increase in NColE7 absorbance and the decrease in azide absorbance confirm that the immobilization is highly specific and covalent.

NColE7 can capture Im7 fusion proteins such as Fab-Im7 constructs with ultrahigh affinity ($K_D \approx 10^{-14}$−10^{-15} M) (Figure S3). Importantly, the NColE7-Im7 interaction can be fully reversed by high salt or low pH elution, enabling controlled regeneration of the sensing surface. All chemical steps, including silanization, peptide blocking, and protein immobilization were performed directly in the ATR flow-through system, allowing continuous spectral monitoring during surface construction.

Optimization by Site-Directed Binding

Since NHS labeling targets lysine residues nonspecifically, the resulting NColE7 layer contains heterogeneously oriented

https://doi.org/10.1021/acs.analchem.6c00250
Anal. Chem. 2026, 98, 11935−11943

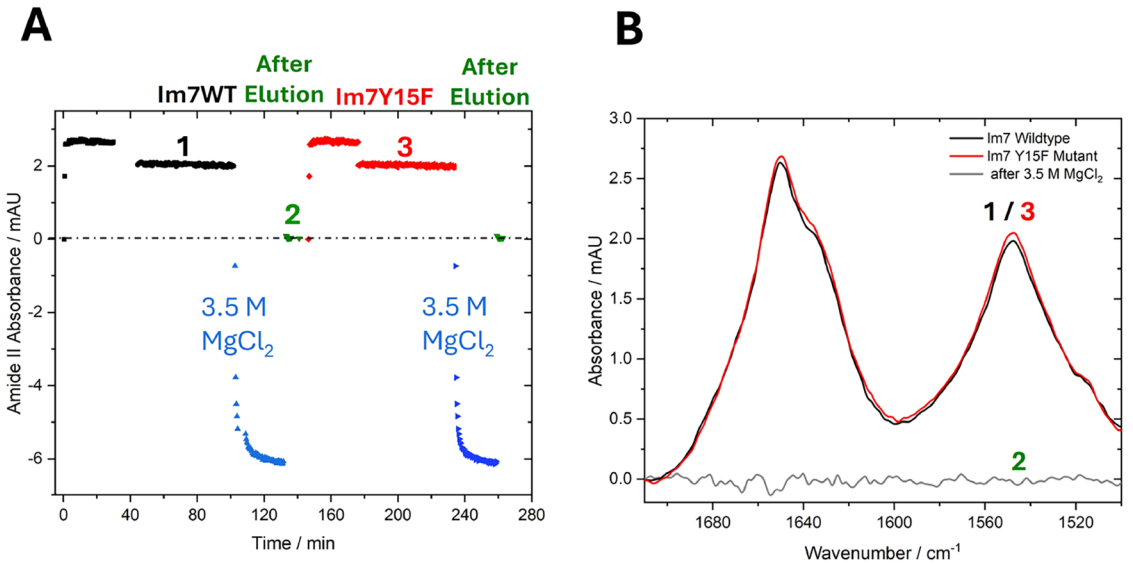

Figure 4. A reversible measurement concept toward difference spectroscopy of two proteins. (A) Kinetic representation of a measurement sequence of two alternating Im7 proteins. First, Im7 WT (black), is bound to an NColE7cys-functionalized surface. This is followed by a 60 min wash phase (1), during which spectra of the bound proteins are recorded. Im7-WT is then eluted from the surface with a 20 min 3.5 M $MgCl_2$ elution step. New spectra were recorded after the regeneration step (2) as a control for the complete wash-off. This is followed by a second binding cycle with an Im7-Y15F mutant (red), again followed by a 60 min wash phase (3). (B) Averaged Im7 spectra after 1 h of spectrum recording before elution and spectra after the elution step (gray) for (WT in black (1) and red for Y15F (3)). Twenty minutes of elution with 3.5 M $MgCl_2$ completely removes Im7 from NColE7 (2).

molecules, some of which orient their Im7-binding pocket in sterically restricted geometries, rendering them inaccessible for binding. To improve the amount of functional oriented NColE7, a site-directed immobilization strategy was developed. A cysteine was introduced into NColE7 via a point mutation at residue 454. This amino acid is located on the opposite side of the Im7 binding pocket, ensuring favorable alignment of NColE7 on the surface. Since there are no other cysteines present in NColE7, the added cysteine enables site-directed coupling via maleimide chemistry using a DBCO-maleimide-linker. This contrasts with the nonselective NHS-based approach and promotes uniform presentation of the Im7-binding site.

To compare the two surfaces, we bound FabIm7 at high concentrations, close to saturation, to both surfaces (Figure S4). We calculated the percentage P of active NColE7 by the amide II absorbance ratios of FabIm7 and NColE7, corrected by the ratio of the amount of amide bonds within these proteins (Formula 1), assuming comparable molar extinction coefficients of the amide II band for both proteins. The calculation with the amide II absorptions A_{amideII}(FabIm7) and A_{amideII}(NcolE7) as determined in Figure S4 yields 76% active NColE7 for the randomly oriented NColE7 and 87% for the oriented $\text{NColE7}_{\text{Cys}}$.

$$P = \frac{A_{\text{amideII}}(\text{FabIm7})}{A_{\text{amideII}}(\text{NColE7})} \times \frac{N_{\text{NHCO}}(\text{NColE7})}{N_{\text{NHCO}}(\text{FabIm7})} \quad (1)$$

$$P_{\text{NColE7}} = \left(\frac{11.2}{4.0} * \frac{148}{546}\right) * 100\% = 75.9\%$$

$$P_{\text{NColE7,Cys}} = \left(\frac{11.9}{3.7} * \frac{148}{546}\right) * 100\% = 87.2\%$$

This shows that site-specific anchoring significantly enhances the functionality of immobilized NColE7. Further, the maleimide-cysteine coupling strategy is much easier to reproduce, since minor changes in labeling conditions (like pH or concentrations) lead to quite different amounts (and possibly positions) of DBCO in the case of the NHS coupling. Thus, cysteine-directed modification was used in all subsequent experiments.

Repeated Washing and Binding Cycles

To assess its applicability in an immuno-IR context, the reversible NColE7-Im7 interface was employed with Im7-Fab fusion constructs derived from the anti-amyloid-β antibody solanezumab and its inactive solanezumab-hcG95A mutant, which served as the functional recognition elements of the sensor.[30] The experiment was designed to show that the same ATR crystal can be used repeatedly to bind proteins, fully regenerate the surface, and subsequently bind another protein without loss of surface performance.

Figure 3A shows 13 consecutive binding-regeneration cycles in which SolanezumabWT-Im7 (black) and Solanezumab-hcG95A-Im7 (pink) were alternately immobilized on the same ATR crystal. In every cycle, ~8 mAU of Fab−Im7 were consistently bound, independently of which fusion protein was used. No decrease in signal amplitude or binding rate was observed throughout the entire 32-h long experiment, demonstrating that the NColE7 anchoring layer retains full binding competence and structural stability even after hours of extensive reuse.

After cycles 1, 10, and 13, antigen-binding activity was assessed by injecting GST-Aβ_{13-28} (green). The antigen spectra were nearly identical in amplitude and shape, confirming that repeated Fab-Im7 binding and regeneration did not impair antigen recognition. The Im7-Fab layer can be removed completely with 3.5 M $MgCl_2$, and each subsequent cycle produces a spectrally almost indistinguishable Fab-Im7 fingerprint (Figure 3B, (1)). Likewise, the regeneration spectra (2) display no detectable amide absorption, indicating

https://doi.org/10.1021/acs.analchem.6c00250
Anal. Chem. 2026, 98, 11935−11943

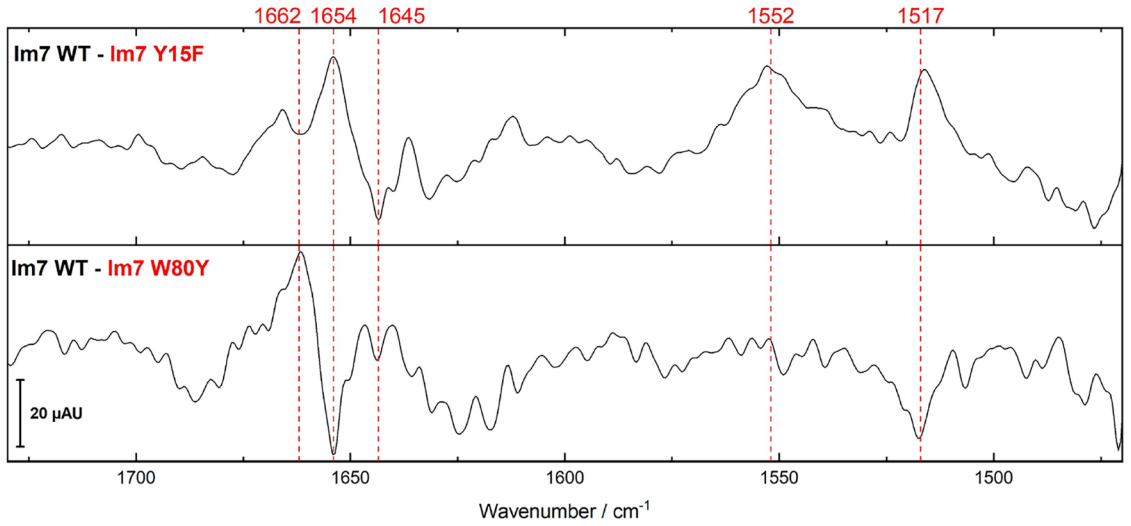

Figure 5. Difference spectrum of Im7-WT − Im7-Y15F and Im7-WT − Im7-W80Y. The shown difference spectra represent the mean of 11 single-cycle subtractions as shown in Figure 4. The Im7-WT − Im7-Y15F spectrum (top box) illustrates the absorbance differences between the wildtype protein and the tyrosine to phenylalanine mutant and reveals prominent positive bands at 1517, 1552, and 1654 cm^{-1}. In contrast, the Im7-WT − Im7-W80Y spectrum (bottom box) displays negative absorbances at 1517 and 1654 cm^{-1} and a positive band 1662 cm^{-1}. The inversion of the 1517 cm^{-1} band reflects the absence or introduction of a tyrosine residue in the respective mutants and provides direct information on the underlying side chain vibration. In addition, both mutations induce shifts within the amide I region, especially at 1654 cm^{-1}, suggesting that the altered residues modify local backbone interactions, likely within the neighboring α-helix segment.

complete elution of bound material and a chemically clean surface for the next cycle.

This highly reproducible and contamination-free regeneration behavior is a fundamental advancement over classical immuno-IR approaches that rely on irreversible antibody coupling. In contrast to such static surfaces, the reversible immuno-IR sensor allows different antibody constructs to be immobilized sequentially on the very same ATR crystal, under truly identical chemical and geometric conditions. As demonstrated in Figure 3C, even after 13 cycles and multiple antibody variants, the antigen can still be measured reliably and with unchanged spectral quality.

The ability to alternately immobilize, measure, and fully remove different Fab-Im7 constructs in rapid succession transforms the system into a powerful screening platform. Antibody fragments with different binding properties, affinity mutations, epitope variants or engineering modifications can be compared directly on the same surface without chip-to-chip variability. This creates a highly controlled analytical environment in which binding behavior, antigen recognition, and spectral differences can be quantified quickly and with minimal material consumption.

Difference Spectroscopy between Different Samples

To demonstrate the sensitivity of the NColE7-based sensing surface, two model proteins; wild-type Im7 (protein A) and a mutant Im7 variant (protein B) were used in alternating binding and elution cycles (Figure 4). The experiment was designed to evaluate whether difference spectroscopy between the binding cycles of both proteins is feasible and if the sensitivity of the technique is high enough to resolve single amino acid exchanges.

Figure 4A displays the amide II kinetics of alternating binding and regeneration cycles using two model proteins, Im7 wildtype (protein A) and an Im7 mutant (protein B). Upon injection of protein A, the amide II band increased rapidly and reached a stable plateau (phase 1), demonstrating efficient binding to the immobilized NColE7 layer. Subsequent elution with 3.5 M $MgCl_2$ immediately returned the signal to baseline (phase 2), confirming complete dissociation of the NColE7-Im7 complex under high-salt conditions. The stable post-elution baseline indicates that the underlying covalently attached REoB-NColE7 architecture remains intact and unaffected by repeated regeneration cycles.

Immediately after regeneration, protein B was introduced into the same flow cell and produced an amide II response of comparable amplitude and stability, reflecting its specific binding to the NColE7 layer. Elution again removed the protein completely, restoring the baseline to its initial level. Repetition of this alternating procedure produced nearly identical binding and elution profiles for both proteins, highlighting the robustness of the reversible sensing platform.

Figure 4B provides the corresponding spectral information. The averaged spectrum from the 60 min binding phase (1) displays the characteristic amide I and II features of the bound Im7 protein. After 20 min of regeneration with 3.5 M $MgCl_2$, the spectrum returns to a flat baseline (2), confirming the quantitative removal of protein without detectable residual material. This complete reset of the sensing surface enables multiple consecutive measurements on the same ATR crystal without cross-contamination, performance drift, or surface aging.

To evaluate the sensitivity of the reversible sensor, difference spectra were generated pairwise for each alternating Im7-WT and Im7 mutant cycle. The difference spectra shown in Figure 5 represent the average of 11 wildtype mutant subtraction cycles recorded on the same ATR crystal. The Im7-WT − Im7-Y15F difference spectrum (Figure 5, top) exhibits positive bands at 1517, 1552, and 1654 cm^{-1}, reflecting tyrosine side-chain vibrations and local backbone perturbations present in the wildtype but absent in the Phe mutant.[2,9] In contrast, the Im7-WT − Im7-W80Y spectrum (Figure 5, bottom) displays negative bands at 1517 and 1654 cm^{-1} and a positive feature at 1662 cm^{-1}. The sign inversion of the 1517 cm^{-1} band directly

https://doi.org/10.1021/acs.analchem.6c00250
Anal. Chem. 2026, 98, 11935−11943

reports whether a Tyr residue is removed or introduced by the mutation, demonstrating that the platform resolves predictable, residue-specific vibrational contributions rather than unspecific global changes.[2]

The mutation-derived amplitudes are on the order of ∼20 μAU. Given that Im7 consists of ∼ 100 amino acids, a single substitution corresponds to ∼1% of the protein. In these measurements, Im7 was bound to the surfaces, which corresponded to a spectral absorption of 2 mAU. For a typical 2 mAU absorbance of the bound protein, a 1% effect corresponds to 20 μAU, which matches the experimentally observed difference signals. Thus, the method effectively operates at the theoretical sensitivity limit required to detect the vibrational contribution of a single amino acid substitution. The accompanying shifts in the amide I region further indicate subtle perturbations of α-helical elements around the mutation site, showing that both side-chain and backbone responses can be captured.

While these results demonstrate residue-level sensitivity, it is important to acknowledge that Im7 is a relatively small, rigid and well-folded model protein. The point mutations investigated here involve tyrosine, a particularly strong and clearly distinguishable vibrational reporter, especially at ∼1517 cm^{-1}. These characteristics make Im7 an analytically favorable test system.

However, these limitations can be mitigated by using advanced data analysis and instrument strategies. Multivariate curve resolution-alternating least-squares (MCR-ALS) can be used to disentangle overlapping components and isolate mutation-specific contributions.[15,34] In addition, increasing the number of WT mutant cycles could increase averaging depth, resulting in an increased signal-to-noise ratio. Furthermore, the choice of internal reflection element is not limited to silicon. The use of germanium could broaden the spectral window and improve sensitivity in regions characteristic of specific side chain modes.

Taken together, while Im7 provides an ideal proof-of-principle system, the underlying reversible ATR-FTIR platform has clear conceptual potential for extension to larger protein systems and more complex biochemical questions.

METHODS

ATR-FTIR Spectroscopy

The silicon IRE was integrated into a Fourier transform infrared (FTIR) Vertex 80 V spectrometer (Bruker Optics, Ettlingen, Germany) in conjunction with a liquid nitrogen-cooled mercury cadmium telluride (MCT) detector and a mid-infrared (MIR) source. The device setup and spectrometer parameters for spectral acquisition have been previously described in detail. The ATR unit (Specac Ltd., Slough, UK) was installed in the sample compartment of the FTIR instrument and aligned at an incidence angle of 45°. Measurements were conducted under continuous flushing with dry air to eliminate the sharp atmospheric water vapor absorbance bands. Baseline and water vapor corrections were performed for all spectra using the standard baseline regions (2710−2690 and 1860−1850 cm^{-1}). For visualization of the azide band, however, a local baseline correction was applied. A linear regression was fitted to spectral regions directly adjacent to the azide band, and the resulting function was subtracted from the spectrum.

We used an improved functionalization method as described in patents WO2024003213A1 and WO2024003214A3 and published elsewhere, where the covalent surface modification and peptide-based blocking layer are described.[16,17,33] Briefly, the initial linker molecule (L1) incorporates a triethoxysilane functional group, enabling covalent attachment to the silicon ATR surface (Figure 1). Subsequent modification steps utilize either strain-promoted azide−alkyne cycloaddition (SPAAC) chemistry, specifically the reaction of aza-dibenzocyclooctyne (DBCO) with azide groups (L2) or the coupling of *N*-hydroxysuccinimide (NHS) esters with primary amines. All functionalization steps were conducted within the flow-through system of the spectrometer, permitting real-time monitoring of each reaction. The resulting surface architecture comprises a covalently immobilized blocking layer, to which the catcher molecule is also covalently attached.

As the primary approach, NColE7 was randomly conjugated to available primary amines using a DBCO-NHCO-PEG13-NHS-Ester (L3) (BroadPharm, San Diego, USA). In the optimized setup, the $NColE7_{cys454}$ was site-directedly coupled with the EZ-Link maleimide-PEG4-DBCO-linker (L3) (Thermo Fisher Scientific, Waltham, USA) according to the manufacturer's instructions.

The ATR crystal surface was functionalized with NColE7 by circulating 50 μg protein in 50 mM MES buffer (0.05% Tween-20, pH 5.5) for 30 min. Unbound NColE7, which may associate the surface noncovalently, was removed by washing with 10x PBS for 20 min. Subsequently, Im7 fusion proteins (e.g., Solanezumab-Im7) or Im7 variants were immobilized on the NColE7 layer. In each case, 40 μg of the respective Im7 construct was circulated in 100 μL MES buffer (50 mM MES + 0.05% Tween-20, pH 5.5) over the surface.

For the illustration of the capabilities of a reversible ATR-FTIR surface (Figure 3), GST-$Aß_{13-28}$ was measured at three independent time points. For this purpose, 1 μg of GST-$Aß_{13-28}$ in 100 μL PBS (pH 7.4) was circulated over the surface for 30 min, followed by a 30 min wash with PBS (pH 7.4). All surface-associated steps were monitored by recording infrared spectra throughout the procedure, enabling precise control over each reaction stage.

Difference Spectroscopy with Im7 Constructs

For difference spectroscopy of two Im7 variants, the two protein constructs were alternately immobilized on and removed from the functionalized IRE using a single flow channel. Each measurement series consisted of 12 consecutive binding-regeneration cycles. For each cycle, 40 μg of the respective Im7 variant in 100 μL MES buffer (50 mM MES + 0.05% Tween-20, pH 5.5) was automatically circulated over the NColE7-functionalized surfaces for 30 min. Unbound protein was removed by washing with 10 x PBS for 10 min, after which the system was returned to MES buffer and spectra of the Im7 layer were recorded for 60 min. Data between 4000 and 900 cm^{-1} were collected with a spectral resolution of 2 cm^{-1} in the double-sided forward−backward data acquisition mode with a scanner speed of 60 kHz. For the Fourier transformation, a zero-filling factor of 4 and Blackmann-Harris 3-term apodization was applied. Spectra were recorded every 20 s. For difference spectroscopy, 100 consecutive spectra were averaged. To release the bound Im7 and regenerate the NColE7 surface, the flow cell was washed with $MgCl_2$ (3.5 M) for 20 min. Afterwards, the system was equilibrated again to MES buffer (5 min). A new background was taken, and the next cycle was initiated. In total, 12 cycles were performed for each pairwise comparison: The measurement was done for Im7-Y15F vs Im7-W80Y, Im7-WT vs Im7Y15F and Im7-WT vs Im7-W80Y.

Calculation of Infrared Difference Spectra

From the wash phases of each binding-regeneration cycle, the mean single-channel (SC) spectra of all 12 Im7 cycles were calculated. Difference absorbance spectra ΔA were obtained by applying the Lambert−Beer relation:

$$\Delta A = -\lg\frac{I_{WT}}{I_{mutant}} \vee \Delta A = -\lg\frac{I_{mutant}}{I_{WT}}$$

where I_{WT} denotes the single-channel spectrum of the Im7 wildtype construct and I_{mutant} denotes the corresponding spectrum of the Im7 mutant. The appropriate ratio was chosen depending on the subtraction direction, required to generate wildtype mutant or mutant-wildtype difference spectra.

https://doi.org/10.1021/acs.analchem.6c00250
Anal. Chem. 2026, 98, 11935−11943

Because the measurement sequence alternated between wild-type and mutant Im7 constructs, difference spectra were always calculated between spectra recorded in closest temporal proximity, thereby minimizing baseline drift and gradual surface changes at the ATR interface. This procedure resulted in 11 individual WT mutant difference spectra, which were averaged resulting in the final WT mutant difference spectra.

Protein Expression and Purification of NColE7 Constructs

The gene encoding Colicin NColE7 (UniProt: Q47112) was cloned into a pET24a expression vector. A T454C substitution was introduced to enable site-specific conjugation, and histidine 545 was mutated to alanine to abolish DNase activity, as described.[35] Both NcolE7 variants (wildtype and $E7_{cys}$) were expressed using the same protocol.

Chemically competent *E. coli* BL21-AI (One Shot) cells were transformed with 100 ng plasmid DNA and plated onto LB agar supplemented with kanamycin (50 μg/mL). Several colonies were used to inoculate 10 mL LB precultures containing kanamycin (50 μg/mL), which were incubated overnight at 37 °C with shaking (220 rpm). These cultures were used to inoculate 5 L of Terrific Broth (TB) medium to an initial OD_{600} of 0.05. Cells were grown at 37 °C with shaking at 80 rpm until mid-log phase (OD_{600} = 0.6−0.8). Protein expression was induced with 0.02% (w/v) L-arabinose and 1 mM IPTG, followed by incubation at 25 °C for 16 h.

Cells were harvested by centrifugation (5000*g*, 15 min, 4 °C) and resuspended in PBS (pH 7.4; 10 mL/L of culture). Cell lysis was performed using five passes through a microfluidizer at 1000 bar. The lysate was clarified by centrifugation (45,000*g*, 1 h, 4 °C), yielding a soluble (cytoplasmic) fraction and an insoluble pellet. The supernatant was passed through a 0.2 μm filter and applied to a nickel-affinity chromatography column (HisTrap) via the engineered His-tag. Bound protein was eluted using a linear imidazole gradient, with elution occurring at approximately 25% imidazole, followed by size exclusion chromatography on a HiLoad 26/60 Superdex 75 pg column (GE Healthcare) at a flow rate of 1 mL min^{-1}.

Expression of Solanezumab-Im7

Solanezumab-Im7 fusion constructs were generated as described previously (Scherlo 2025).[30] The Im7 gene (UniProt Q03708) was fused to the 3′ end of the solanezumab light chain via a flexible peptide linker ($(G_4S)_2$-GGRAS). Both, the wild-type Solanezumab-Im7 fusion protein and the inactive Im7 mutant (G95A) were produced under identical expression conditions.

Plasmid DNA encoding the respective construct was transformed into *E. coli* BL21-AI (One Shot) cells. Transformants were used to inoculate LB precultures supplemented with kanamycin (50 μg/mL), which were incubated overnight at 37 °C with shaking. For large-scale expression, 5 L of Terrific Broth (TB) medium was inoculated to an initial OD_{600} of 0.05. Cultures were grown at 37 °C until mid-log phase (OD_{600} = 0.6−0.8), at which point expression was induced with 0.02% (w/v) L-arabinose and 1 mM IPTG. Following induction, the temperature was decreased to 18 °C, and cultures were incubated for 40 h with continuous shaking.

Cells were harvested by centrifugation (5000*g*, 15 min, 4 °C) and resuspended in PBS (pH 7.4; 10 mL/L culture). Lysis was performed using five passes through a microfluidizer at 1000 bar. The lysate was clarified by centrifugation (45,000*g*, 1 h, 4 °C) to obtain the soluble cytoplasmic fraction. The supernatant was passed through a 0.2 μm filter and subjected to sequential affinity chromatography. First, His-tag affinity purification (HisTrap) targeting the heavy chain was performed, followed by Strep-tag affinity purification (StrepTrap HP) targeting the light chain. The resulting Fab-Im7 fusion proteins, containing both affinity tags, were finally polished by size-exclusion chromatography.

Expression and Purification of GST-Aβ_{13-28}

To characterize the Im7-Fab fusion proteins, a glutathione S-transferase (GST)-Aβ_{13-28} fusion protein was generated in *E. coli*. The GST domain from *S. japonicum* was fused to the N-terminus of the Aβ_{13-28} peptide, and the corresponding gene construct was expressed heterologously in *E. coli*. Plasmid DNA encoding the fusion protein was transformed into *E. coli* BL21-AI (One Shot) cells. Transformants were used to inoculate LB precultures supplemented with kanamycin (50 μg/mL), which were incubated overnight at 37 °C with shaking.

For large-scale expression, 5 L of Terrific Broth (TB) medium was inoculated to an initial OD_{600} of 0.05 and grown at 37 °C until mid-log phase (OD_{600} = 0.6−0.8). Expression was induced with 0.02% (w/v) L-arabinose and 1 mM IPTG, after which the incubation temperature was reduced to 30 °C and cultures were shaken for 16 h.

Cells were harvested by centrifugation (5000*g*, 15 min, 4 °C) and resuspended in PBS (pH 7.4; 10 mL/l culture). Lysis was performed using five passes through a microfluidizer at 1000 bar. The lysate was clarified by centrifugation (45,000*g*, 1 h, 4 °C), yielding a soluble cytoplasmic fraction, which was filtered through a 0.2 μm membrane and subjected to affinity purification. GST-tag affinity chromatography (GST HiTrap) was performed using glutathione Sepharose resin to isolate the GST-Aβ_{13-28} fusion protein, followed by size exclusion chromatography on a HiLoad 26/60 Superdex 75 pg column (GE Healthcare) at a flow rate of 1 mL min^{-1}.

Expression of Im7-WT, Im7-W80Y, Im7-Y15F

The Im7 plasmids used contain the Im7 sequence (Uniprot.Q03708) and a C-terminal Deca-His tag, which are connected via a GSESK linker. The same expression protocol was used for all three constructs. For this purpose, the respective plasmid DNA was transformed into *E. coli* BL21-AI (One Shot) cells, which were subsequently grown in LB precultures with kanamycin (50 μg/mL) overnight at 37 °C with shaking. For expression, 5 L of TB medium was inoculated at an OD_{600} of 0.05 at 37 °C and induced at an OD600 of 0.6−0.8 with 0.02% arabinose and 1 mM IPTG. From the time of induction, the temperature was reduced to 25 °C, and the cultures were incubated for 16 h with constant shaking. After overexpression was complete, the cells were spun down (5000*g*, 15 min, 4 °C) and resuspended in 10 mL/l PBS (pH 7.4). The cells were then disrupted via five passages through a microfluidizer (pressure 1000 bar). The resulting material was centrifuged (45,000*g*, 1 h, 4 °C) and separated into two components: the soluble fraction in the supernatant (cytoplasmic fraction) and the insoluble fraction in the sediment. The supernatant was then filtered (pore size of 0.2 μm) and purified via affinity chromatography. For purification, we used His-Tag affinity chromatography (HisTrap HP) followed by size-exclusion chromatography as described above.

■ ASSOCIATED CONTENT

Supporting Information

The Supporting Information is available free of charge at https://pubs.acs.org/doi/10.1021/acs.analchem.6c00250.

Figures S1−S4 and calculation of the surface concentration (PDF)

■ AUTHOR INFORMATION

Corresponding Author

Carsten Kötting − *Center for Protein Diagnostics (PRODI), Biospectroscopy and Department of Biophysics, Ruhr University Bochum, 44780 Bochum, Germany;* orcid.org/0000-0002-3599-9657; Email: carsten.koetting@rub.de

Authors

Adrian Höveler − *Center for Protein Diagnostics (PRODI), Biospectroscopy and Department of Biophysics, Ruhr University Bochum, 44780 Bochum, Germany;* orcid.org/0009-0008-3039-1555

Marvin Mann − *Center for Protein Diagnostics (PRODI), Biospectroscopy and Department of Biophysics, Ruhr*

https://doi.org/10.1021/acs.analchem.6c00250
Anal. Chem. 2026, 98, 11935−11943

University Bochum, 44780 Bochum, Germany; orcid.org/0009-0006-3183-9011

Maiko Czarnetzki − *Center for Protein Diagnostics (PRODI), Biospectroscopy and Department of Biophysics, Ruhr University Bochum, 44780 Bochum, Germany*

Jonas Simon − *Center for Protein Diagnostics (PRODI), Biospectroscopy and Department of Biophysics, Ruhr University Bochum, 44780 Bochum, Germany;* orcid.org/0009-0005-4912-7146

Nicolai Marpert − *Center for Protein Diagnostics (PRODI), Biospectroscopy and Department of Biophysics, Ruhr University Bochum, 44780 Bochum, Germany*

Jörn Güldenhaupt − *Center for Protein Diagnostics (PRODI), Biospectroscopy and Department of Biophysics, Ruhr University Bochum, 44780 Bochum, Germany*

Klaus Gerwert − *Center for Protein Diagnostics (PRODI), Biospectroscopy and Department of Biophysics, Ruhr University Bochum, 44780 Bochum, Germany*

Complete contact information is available at: https://pubs.acs.org/10.1021/acs.analchem.6c00250

Author Contributions

[§]A.H. and M.M. contributed equally to this work.

Notes

The authors declare the following competing financial interest(s): K.G. is the founder and CEO of betaSENSE GmbH. The remaining authors declare no competing interests.

■ ACKNOWLEDGMENTS

We thank Kristin Labudda for help with the expression and purification of Im7.

■ REFERENCES

(1) Kötting, C.; Gerwert, K. Proteins in action monitored by time-resolved FTIR spectroscopy. *ChemPhysChem* **2005**, *6* (5), 881−888.

(2) Barth, A. Infrared spectroscopy of proteins. *Biochim. Biophys. Acta* **2007**, *1767* (9), 1073−1101.

(3) Goormaghtigh, E.; Ruysschaert, J.-M.; Raussens, V. Evaluation of the information content in infrared spectra for protein secondary structure determination. *Biophys. J.* **2006**, *90* (8), 2946−2957.

(4) Nabers, A.; Ollesch, J.; Schartner, J.; Kötting, C.; Genius, J.; Hafermann, H.; Klafki, H.; Gerwert, K.; Wiltfang, J. Amyloid-β-Secondary Structure Distribution in Cerebrospinal Fluid and Blood Measured by an Immuno-Infrared-Sensor: A Biomarker Candidate for Alzheimer's Disease. *Anal. Chem.* **2016**, *88* (5), 2755−2762.

(5) Beyer, L.; Stocker, H.; Rujescu, D.; Holleczek, B.; Stockmann, J.; Nabers, A.; Brenner, H.; Gerwert, K. Amyloid-beta misfolding and GFAP predict risk of clinical Alzheimer's disease diagnosis within 17 years. *Alzheimers Dement.* **2023**, *19* (3), 1020−1028.

(6) Stockmann, J.; Verberk, I. M. W.; Timmesfeld, N.; Denz, R.; Budde, B.; Lange-Leifhelm, J.; Scheltens, P.; van der Flier, W. M.; Nabers, A.; Teunissen, C. E.; Gerwert, K. Amyloid-β misfolding as a plasma biomarker indicates risk for future clinical Alzheimer's disease in individuals with subjective cognitive decline. *Alzheimers Res. Ther.* **2020**, *12* (1), 169.

(7) Schuler, M.; Gerwert, G.; Mann, M.; Woitzik, N.; Langenhoff, L.; Hubert, D.; Duman, D.; Höveler, A.; Galkowski, S.; Simon, J.; Denz, R.; Weber, S.; Kwon, E.-H.; Wanka, R.; Kötting, C.; Güldenhaupt, J.; Beyer, L.; Tönges, L.; Mollenhauer, B.; Gerwert, K. Alpha-synuclein misfolding as fluid biomarker for Parkinson's disease measured with the iRS platform. *EMBO Mol. Med.* **2025**, *17* (6), 1203−1221.

(8) Langenhoff, L.; Simon, J.; Weber, S.; Hubert, D.; Schuler, M.; Mann, M.; Puzovic, V.; Gerwert, G.; Hoeveler, A.; Beyer, L.; Toenges, L.; Koetting, C.; Gueldenhaupt, J.; Mollenhauer, B.; Gerwert, K. Misfolding of Alpha-synuclein as Blood-based Biomarker for Parkinson's Diesease *MedRxiv* 2025; Vol. *21* 12 DOI: 10.64898/2025.12.19.25342662.

(9) Lorenz-Fonfria, V. A. Infrared Difference Spectroscopy of Proteins: From Bands to Bonds. *Chem. Rev.* **2020**, *120* (7), 3466−3576.

(10) Zscherp, C.; Barth, A. Reaction-induced infrared difference spectroscopy for the study of protein reaction mechanisms. *Biochemistry* **2001**, *40* (7), 1875−1883.

(11) Gerwert, K.; Souvignier, G.; Hess, B. Simultaneous monitoring of light-induced changes in protein side-group protonation, chromophore isomerization, and backbone motion of bacteriorhodopsin by time-resolved Fourier-transform infrared spectroscopy. *Proc. Natl. Acad. Sci. U.S.A.* **1990**, *87* (24), 9774−9778.

(12) Kazarian, S. G.; Chan, K. L. A. ATR-FTIR spectroscopic imaging: recent advances and applications to biological systems. *Analyst* **2013**, *138* (7), 1940−1951.

(13) Rich, P. R.; Iwaki, M. Methods to probe protein transitions with ATR infrared spectroscopy. *Mol. BioSyst.* **2007**, *3* (6), 398−407.

(14) Mann, D.; Güldenhaupt, J.; Schartner, J.; Gerwert, K.; Kötting, C. The protonation states of GTP and GppNHp in Ras proteins. *J. Biol. Chem.* **2018**, *293* (11), 3871−3879.

(15) Güldenhaupt, J.; Amaral, M.; Kötting, C.; Schartner, J.; Musil, D.; Frech, M.; Gerwert, K. Ligand-Induced Conformational Changes in HSP90 Monitored Time Resolved and Label Free-Towards a Conformational Activity Screening for Drug Discovery. *Angew. Chem., Int. Ed.* **2018**, *57* (31), 9955−9960.

(16) Güldenhaupt, J.; Mann, M.; Woitzik, N.; Langenhoff, L. C.; Budde, B.; Gerwert, G.; Kötting, C.; Gerwert, K. Molecular Probe Functionalized Element. European Patent EP20220182414, June 30, 2022.

(17) Mann, M.; Langenhoff, L. C.; Güldenhaupt, J.; Wanka, R.; Kötting, C.; Gerwert, K. Surface Functionalized Optical Element.European Patent EP20220182415, June 30, 2022.

(18) Rich, R. L.; Myszka, D. G. Advances in surface plasmon resonance biosensor analysis. *Curr. Opin. Biotechnol.* **2000**, *11* (1), 54−61.

(19) Homola, J. Surface plasmon resonance sensors for detection of chemical and biological species. *Chem. Rev.* **2008**, *108* (2), 462−493.

(20) Gershon, P. D.; Khilko, S. Stable chelating linkage for reversible immobilization of oligohistidine tagged proteins in the BIAcore surface plasmon resonance detector. *J. Immunol. Methods* **1995**, *183* (1), 65−76.

(21) Arugula, M. A.; Simonian, A. Novel trends in affinity biosensors: current challenges and perspectives. *Meas. Sci. Technol.* **2014**, *25* (3), No. 032001.

(22) Hirlekar Schmid, A.; Stanca, S. E.; Thakur, M. S.; Thampi, K. R.; Raman Suri, C. Site-directed antibody immobilization on gold substrate for surface plasmon resonance sensors. *Sens. Actuators, B* **2006**, *113* (1), 297−303.

(23) Jia, Y.; Chen, S.; Wang, Q.; Li, J. Recent progress in biosensor regeneration techniques. *Nanoscale* **2024**, *16* (6), 2834−2846.

(24) Schartner, J.; Güldenhaupt, J.; Mei, B.; Rögner, M.; Muhler, M.; Gerwert, K.; Kötting, C. Universal method for protein immobilization on chemically functionalized germanium investigated by ATR-FTIR difference spectroscopy. *J. Am. Chem. Soc.* **2013**, *135* (10), 4079−4087.

(25) Lahcen, A. A.; Amine, A. Biorecognition elements. In *Wearable Physical, Chemical and Biological Sensors*; Elsevier, 2022; pp 41−70 DOI: 10.1016/B978-0-12-821661-3.00011-2.

(26) Ko, T.-P.; Liao, C.-C.; Ku, W.-Y.; Chak, K.-F.; Yuan, H. The crystal structure of the DNase domain of colicin E7 in complex with its inhibitor Im7 protein. *Structure* **1999**, *7*, 91−102.

(27) Li, W.; Keeble, A. H.; Giffard, C.; James, R.; Moore, G. R.; Kleanthous, C. Highly discriminating protein-protein interaction specificities in the context of a conserved binding energy hotspot. *J. Mol. Biol.* **2004**, *337* (3), 743−759.

(28) Juraja, S. M.; Mulhern, T. D.; Hudson, P. J.; Hattarki, M. K.; Carmichael, J. A.; Nuttall, S. D. Engineering of the *Escherichia coli* Im7 immunity protein as a loop display scaffold. *Protein Eng. Des Sel.* **2006**, *19* (5), 231−244.
(29) Hosse, R. J.; Tay, L.; Hattarki, M. K.; Pontes-Braz, L.; Pearce, L. A.; Nuttall, S. D.; Dolezal, O. Kinetic screening of antibody-Im7 conjugates by capture on a colicin E7 DNase domain using optical biosensors. *Anal. Biochem.* **2009**, *385* (2), 346−357.
(30) Scherlo, M.; Höveler, A.; Mann, M.; Gerwert, G.; Güldenhaupt, J.; Gerwert, K.; Rudack, T.; Kötting, C. Replacement of a single residue in an antibody abolishes cognate antigen binding, as predicted by theoretical methods. *Comput. Struct. Biotechnol. J.* **2025**, *27*, 4363−4372.
(31) Vassylyeva, M. N.; Klyuyev, S.; Vassylyev, A. D.; Wesson, H.; Zhang, Z.; Renfrow, M. B.; Wang, H.; Higgins, N. P.; Chow, L. T.; Vassylyev, D. G. Efficient, ultra-high-affinity chromatography in a one-step purification of complex proteins. *Proc. Natl. Acad. Sci. U.S.A.* **2017**, *114* (26), E5138−E5147.
(32) Medipally, H.; Mann, M.; Kötting, C.; van Berkel, W. J. H.; Nowaczyk, M. M. A Clickable Photosystem I, Ferredoxin, and Ferredoxin NADP+ Reductase Fusion System for Light-Driven NADPH Regeneration. *ChemBioChem* **2023**, *24* (14), No. e202300025.
(33) Gerwert, G.; Mann, M.; Langenhoff, L.; Woitzik, N.; Hubert, D.; Duman, D.; Hoeveler, A.; Budde, S.; Simon, J.; Beyer, L.; Schuler, M.; Weber, S.; Mollenhauer, B.; Kötting, C.; Gueldenhaupt, J.; Gerwert, K. An immuno-Infrared Sensor detects preclinical Alzheimer's and Parkinson's Disease by misfolding *arXiv*, Sept 18, 2025 http://arxiv.org/pdf/2509.14972v1.
(34) Jaumot, J.; Gargallo, R.; Juan, A. de.; Tauler, R. A graphical user-friendly interface for MCR-ALS: a new tool for multivariate curve resolution in MATLAB. *Chemom. Intell. Lab. Syst.* **2005**, *76* (1), 101−110.
(35) Doudeva, L. G.; Huang, H.; Hsia, K.-C.; Shi, Z.; Li, C.-L.; Shen, Y.; Cheng, Y.-S.; Yuan, H. S. Crystal structural analysis and metal-dependent stability and activity studies of the ColE7 endonuclease domain in complex with DNA/Zn2+ or inhibitor/Ni2+. *Protein Sci.* **2006**, *15* (2), 269−280.

https://doi.org/10.1021/acs.analchem.6c00250
Anal. Chem. 2026, 98, 11935−11943